DOI: 10.13009/EUCASS2025-537
11TH EUROPEAN CONFERENCE FOR AERONAUTICS AND SPACE SCIENCES (EUCASS)

Experimental characterization of a 15KN LOX/LNG regeneratively cooled combustion chamber with propellant temperature variation

Tomas Cruz[†] [1], *Julian Matt*[1], *Matteo Crachi*[2] , *Stefano Matteini*[3], *Yohann Torres*[3], *Robson dos Santos*[4], *Wolfgang Armbruster*[4]

[1]*The Exploration Company SAS, Bordeaux, France*

[2]*Politecnico di Torino University, Turin, Italy*

[3]*European Space Agency, Noordwijk, Netherlands*

[4]*German Aerospace Center, Institute of Space Propulsion, Lampoldshausen, Germany*

tomas@exploration.space

[†] Corresponding Author

Abstract

This paper presents the results of an experimental test campaign conducted to evaluate the performance of the Huracan LOX/LNG rocket engine's thrust chamber, developed as part of the Nyx Moon vehicle by The Exploration Company, which is a modular, reusable, and refillable space vehicle designed for lunar missions. The third iteration of the Huracan thrust chamber is tested at the German Aerospace Center (DLR) in Lampoldshausen, with support from the European Space Agency (ESA). The test campaign accumulated over 600 seconds of hot-fire testing, with a single test lasting more than 2 minutes. The campaign focuses on the influence of methane injection temperature, controlled by mixing gaseous methane at ambient temperature with cryogenic liquid methane. Variations in chamber pressure and mixture ratio are also investigated. The study aims to assess injector performance, with specific emphasis on combustion efficiency and heat transfer. The results indicate that lower methane temperatures lead to significant reductions in combustion efficiency, due to lower momentum flux ratios and Weber number. Furthermore, a 1D regenerative cooling model is calibrated using the experimental data. These findings contribute to a deeper understanding of injector performance and cooling system modelling of the Huracan engine.

1. Introduction

The Huracan project aims to deliver a cryogenic LOX/LNG propulsion system with reusability, deep-throttling capability, and cost-effective manufacturability. Designed as the main propulsion unit for the Nyx Moon spacecraft, the Huracan engine is intended for mission to and within the cislunar environment, including lunar landing and return trajectories. As part of its modular architecture, Nyx will support a variety of mission profiles, with the Huracan engine at the core of its lunar service module.

Figure 1: Artistic render of the Nyx moon vehicle

DOI: 10.13009/EUCASS2025-537

The Thrust Chamber Assembly (TCA) of the Huracan engine is regeneratively cooled and designed for additive manufacturing. Prior campaigns focused on validating injector designs. These included single element tests [14] as well as water cooled chamber tests to validate the full scale injector head design [13]. The second full scale test campaign introduced regenerative cooling for the first time, with the goal to validate the design of the combustion chamber. During the second full scale campaign it was observed that the heat pickup from the combustion chamber was overpredicted in the calculations, which lead to a mismatch between the regenerative cooling system and the injectors, resulting in lower combustion efficiency than expected.
This paper presents the results of the third hot-fire campaign of the Huracan engine, carried out at DLR's P8 test bench in Lampoldshausen, Germany, with support from the European Space Agency. This campaign featured the third iteration of the regeneratively cooled TCA and a propellant temperature control system to study the impact of fuel temperature on combustion efficiency. Over 600 seconds of cumulative hot-fire time were achieved, including a single test exceeding two minutes. A sequence of 19 rapid thermal cycles was also conducted to evaluate thermomechanical fatigue and reusability, accumulation a total of 35 cycles, five times the target for lunar operations [15].
A central focus of the campaign was the experimental characterization of how varying the methane injection temperature affects combustion performance. By blending ambient temperature CNG with cryogenic LNG, injector performance was assessed at different mixture and chamber pressure conditions. These results not only contribute to refining combustion models but also support the calibration of a 1D regenerative cooling model. With the improved models it will be possible to close the design loop and fine tune the injector design to match the output of the cooling system, thus achieving high combustion efficiency.
The paper is structured as follows: Section 2 describes the experimental setup and test facility; Section 3 outlines the methodology used for data analysis; Section 4 presents the results of the hot-fire testing and cooling analysis; and Section 5 concludes an outlook for further engine development.

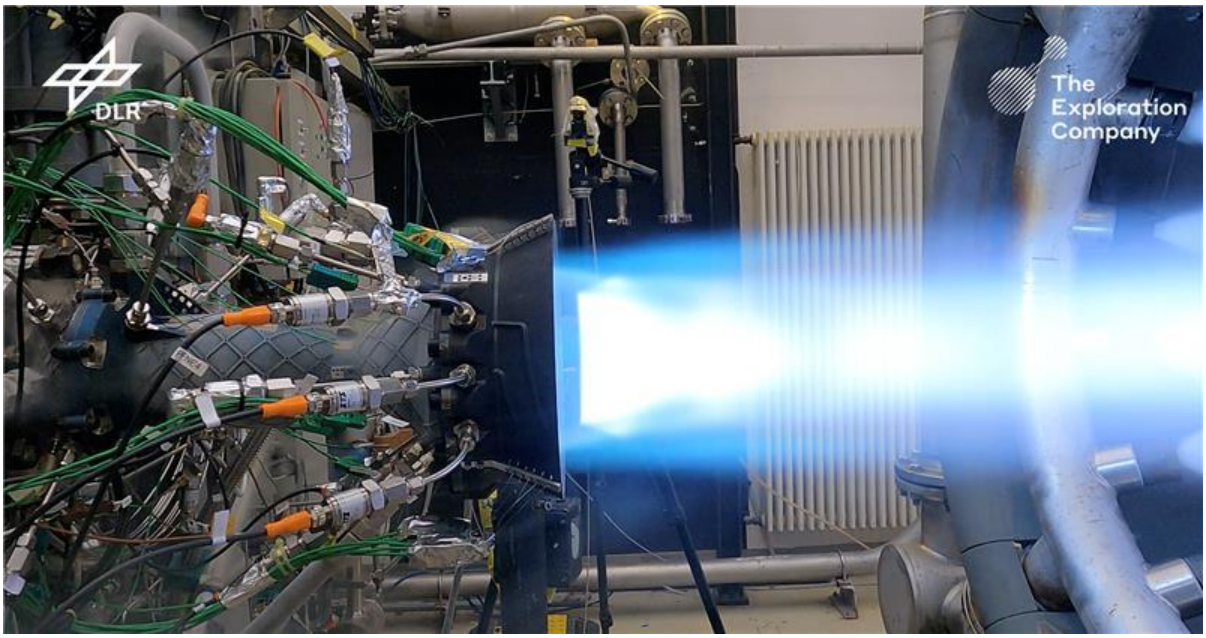

Figure 2: Hot fire test of the third iteration of the Huracan's Thrust Chamber Assembly

2. Experimental Setup

The experimental focus of this campaign had a particular emphasis on controlling the temperature of the methane entering the injector head, since in the previous two campaigns, it was found that this parameter had a significant impact on the combustion efficiency. For this reason, it was required that the setup allowed the decoupling of the injector head feeding and the combustion chamber cooling. The complete test article, including all relevant subsystems, is illustrated in Figure 3.

DOI: 10.13009/EUCASS2025-537

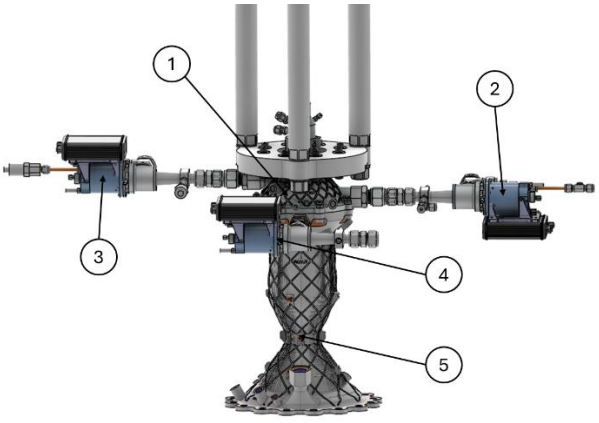

Figure 3: Test article. 1) IH, 2) MFV, 3) MOV, 4) RCV, 5) MCC

The test article consists of an injector head (IH) mounted on top of a regeneratively cooled combustion chamber (MCC), and three control valves, one for the LOX line (MOV), one at the outlet of the regenerative circuit (RCV) and one for the fuel side upstream of the injector head (MFV).
A simplified schematic of the facility's propellant feed system is provided in Figure 4. In this specific configuration, the coolant exiting the regenerative channels does not enter the injector head. Instead it passes through the control valve and then is directed to a dump line. This design choice was made to ensure that the fuel temperature at the injector could be independently controlled and without the influence of the cooling circuit. The RCV control valve is used to regulate the pressure level at the exit of the cooling circuit.

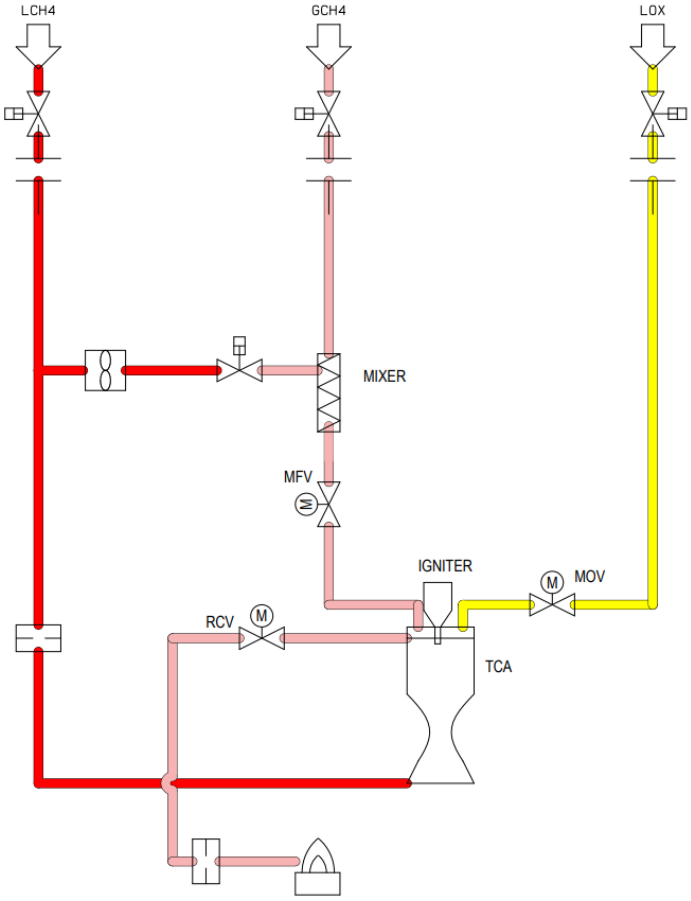

Figure 4: Piping and Interface Document (P&ID)

The LOX feed system was relatively simple, since the LOX was delivered directly from the run tank to the injector head by the mass flow control system of P8. On the other hand, the methane feed system relied on a dual-supply system

DOI: 10.13009/EUCASS2025-537

consisting of cryogenic LNG and ambient temperature CNG. This was necessary to be able to control the injection temperature.
To achieve this, the LNG line was branched into two lines. The primary line, which carried the majority of the LNG mass flow was directed toward the regenerative cooling inlet of the combustion chamber. The secondary line was directed toward a mixer, where the cryogenic LNG was combined with CNG to yield a fuel mixture at the desired temperature. This mixture then passes through the MFV before entering the injector head. The mass flow through this secondary LNG branch was regulated by a dedicated proportional control valve. In parallel, the CNG line was connected to the other inlet of the mixing element. The total mass flow of the LNG and the CNG lines were regulated by bench control valves.
The fuel temperature control strategy relied on an enthalpy balance and it was implemented through a closed-loop mass flow controller on the secondary LNG line, without direct feedback from temperature sensors. This approach, while more susceptible to deviations from the desired outlet temperature, allowed for a relatively simple and fast control strategy.
One particular feature of the set-up was that three out of the four mass flow regulating valves were on the fuel side, which meant that they were hydraulically coupled due to their interconnection caused by the secondary LNG line. This coupling can introduce instabilities into the system. These effects will be discussed further in Section 4.
Thermocouples and pressure transducers were installed at strategic locations throughout the methane feed system and the different subcomponents to monitor the mixing behaviour and well as to characterize the performance of the test article. The sensors were placed at the inlets and outlet of the mixer, at the inlet and outlet manifolds of the regenerative circuit and at the propellant domes of the injector head.

3. Methodology

This section outlines the theoretical foundations of the regenerative cooling model and the detailed procedure used to calculate the combustion efficiency of the thrust chamber assembly. Since experimental combustion efficiency cannot be directly measured, it is inferred by comparing the measured characteristic velocity with a theoretically ideal reference.

3.1 1D Regenerative cooling model

A critical component of the overall performance prediction is the accurate estimation of the regenerative cooling (RC) system's thermal behaviour. To achieve this, a one-dimensional (1D) thermal model was implemented based on well-established framework used in rocket engine cooling analysis such as the one in [3]. The model computes the local heat transfer along the cooling channel, enabling detailed prediction of the wall temperature profile and the evolution of the thermodynamic state of the coolant.
The regenerative cooling system is modelled as a 1D steady-state heat transfer problem, where only radial heat conduction though the chamber wall and bulk fluid properties are considered. The governing equations solved in this model are the conservation equations or mass, momentum and energy applied to a control volume that is discretized along the coolant flow path.
The heat flux from the combustion gases to the chamber wall is computed using the Bartz correlation [12], a widely used semi-empirical correlation that estimates the convective heat transfer coefficient based on local flow conditions. The adiabatic wall temperature is used as the reference temperature for the hot side. Additionally, radiative heat transfer from the gas to the wall is included [11]. The chamber wall is assumed to transfer heat only in the radial direction but the finned geometry of the cooling ribs is accounted for using an analytical fin efficiency model [6]. On the coolant side, the Dittus-Boelter correlation is used to estimate the convective heat transfer coefficient. All hot gas properties are calculated with Cantera [5], while the thermophysical properties of the coolant are calculated with REFPROP [10].
The pressure loss across the cooling channel is computed using the Darcy-Weisbach equation. The friction factor is estimated for turbulent flows using correlations for rough internal surfaces. The equivalent sand grain roughness is derived from the arithmetic roughness average, Ra, using an empirical relationship for additively manufactured channels [1]. The value is adjusted based on experimental pressure drop data to better match actual flow conditions.
To account for empirical deviations from idealised models and manufacturing variability, two empirical correction factors are introduced to correct the hot-side and the cold-side heat transfer coefficient. These factors are calibrated against experimental measurements.
This predictive RC model is used both to analyse test data as well as a design tool for future hardware iterations. The proper validation of the model is therefore essential to the development process of the TCA. Since the configuration of this test campaign did not have a closed regenerative cooling system, this model is also used for the combustion efficiency calculation to take into account the heat loss to the walls.

DOI: 10.13009/EUCASS2025-537

3.2 Combustion efficiency calculation

Combustion efficiency, η^*, is defined as the ratio between the measured characteristic velocity, c^*, observed in the test and its ideal value, where characteristic velocity is defined as the ratio of chamber pressure, p, times the throat area, A_t, to the total mass flow, $\dot{m}$:

$$c^* = \frac{pA_t}{\dot{m}} \tag{1}$$

The ideal characteristic velocity is computed using an equilibrium chemistry solution based on the measured mixture ratio and inlet propellant conditions. The combustion efficiency is a critical metric of a rocket engine, because it quantifies how closely the engine behaviour approaches the ideal thermodynamic performance. This single value encapsulates a wide range of physical inefficiencies and deviations. In the complex environment of a combustion chamber, many mechanisms act to reduce performance compared to the theoretical maximum, including [7]:

- Incomplete mixing or combustion, especially under non-ideal injector conditions
- Heat losses through the chamber walls that reduce the available energy for expansion
- Viscous boundary layer effects, which reduce momentum near the walls
- Flow non-uniformities or 2D flow effects, which further restrict the flow when compared to 1D theory
- Geometric deviations, including throat erosion, thermal-mechanical deformation or manufacturing imperfections

Since it is extremely difficult to isolate and measure each of these losses individually, the combustion efficiency provides a practical and comprehensive way to assess overall engine performance. However, to ensure the efficiency value is meaningful, it is essential to establish a fair comparison between the measured result and the ideal model. For this reason, several correction terms are added to the ideal model, to bring it closer to the real case.

A schematic for the procedure for calculating the combustion efficiency used in this work can be seen in Figure 5 [2]. The calculation of combustion efficiency starts with the known quantities of chamber geometry, specifically the throat area and the contraction ratio, the total propellant mass flows and inlet temperatures. To account for heat loss, the 1D RC model is used to calculated the heat transfer rate between the injector face plate and the throat. This heat is subtracted from the original fuel injection enthalpy. Note that this is an important step, because unlike the usual configuration of the engine, this test campaign was conducted without a fully closed regenerative cooling loop. As a result, the heat absorbed in the cooling circuit does not re-enter the combustion process. Therefore, correcting for this heat loss is necessary to ensure that test points with different cooling conditions can be fairly compared and that combustion efficiency reflects only phenomena related to combustion and flow inside the combustion chamber.

Next, Cantera is used to compute the thermodynamic state of the combustion chamber through an equilibrium solution based on the injected mass flow rates, mixture ratio and the adjusted enthalpies [8]. The ideal total pressure at the injection plane, $p'_{0,inj}$, is calculated iteratively by comparing the measured mass flows with the ones we obtain from the ideal characteristic velocity and throat area. However, because the combustion calculation assumes zero axial momentum at the injector plane, an additional pressure term is added, which is the injected momentum, $u_i\dot{m}_i$ where i denotes the propellant (o for oxidizer and f for fuel), divided by the chamber cross-sectional area, A_c.

$$p_{0,inj} = p'_{0,inj} + \frac{u_f\dot{m}_f}{\mathrm{A_c}} + \frac{u_o\dot{m}_o}{\mathrm{A_c}} \tag{2}$$

To address losses due to irreversible acceleration in the constant-area combustion section, a second combustion calculation is performed, this time using the Finite Area Combustor (FAC) method [9], which yields the static pressure at the beginning of the convergent section, p_{EoC}. With the Mach number, Ma, and the specific heat ratio κ, it is possible to convert the static pressure to the total pressure, $p_{0,EoC}$, using isentropic relations. The same is done to the experimentally measured static pressure.

$$p_{0,EoC} = p_{EoC}\left(1 + \frac{\kappa - 1}{2}Ma^2\right)^{\frac{\kappa}{\kappa-1}} \tag{3}$$

Finally, the combustion efficiency is determined as the ratio of experimental to ideal total pressures. This value captures the combined effects of all loss mechanisms that were described above.

DOI: 10.13009/EUCASS2025-537

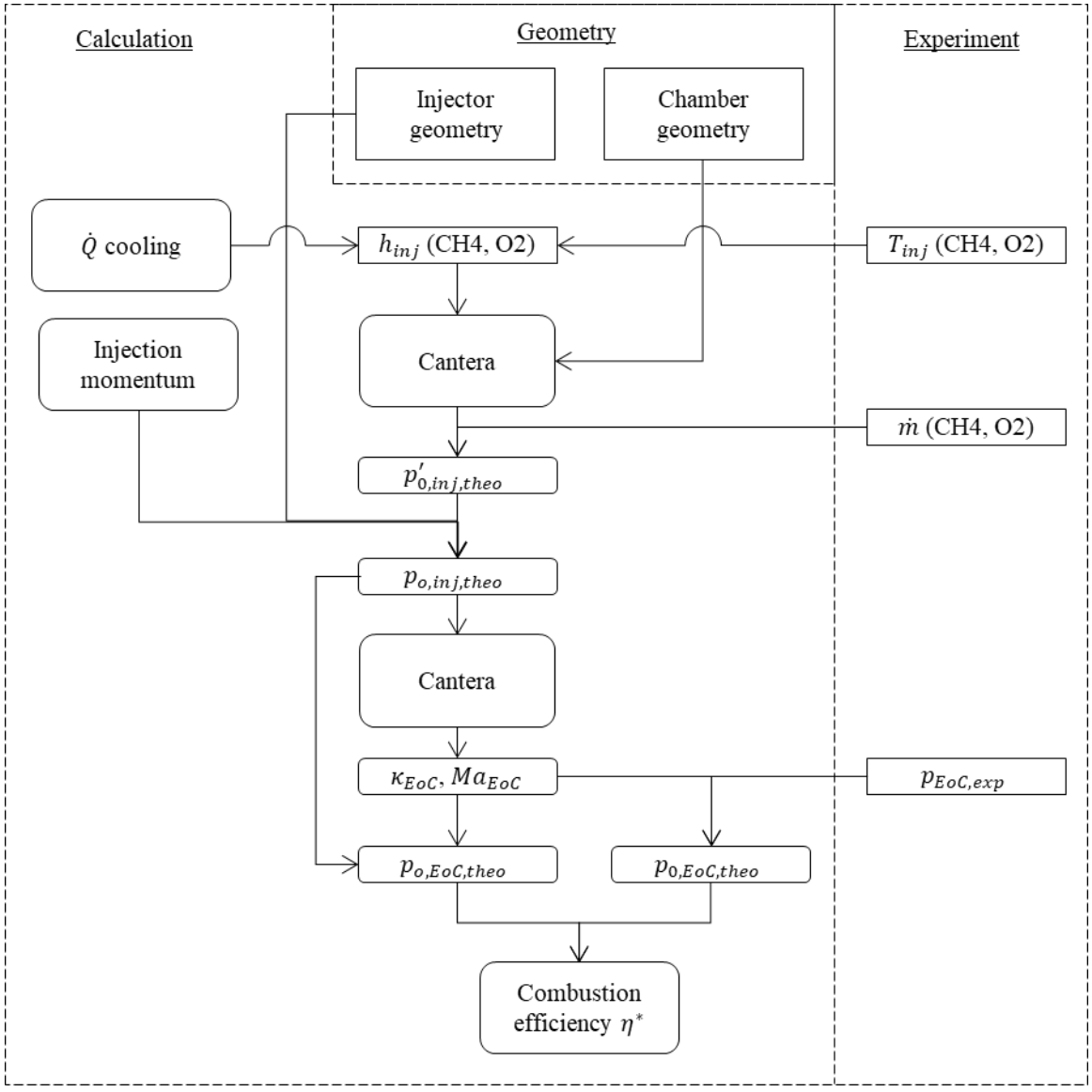

Figure 5: Workflow to estimate the combustion efficiency [2].

4. Results and Discussion

4.1 Experimental domain

The experimental campaign was designed to investigate the combustion performance of the thrust chamber across a wide range of operating conditions. Three main parameters were varied systematically: total mass flow rate, mixture ratio (O/F) and fuel inlet temperature.

The injected mass flow rates were tested at three discrete levels corresponding to 50%, 75% and 100% of the nominal condition. Similarly, the mixture ratio was varied by ±6% around the nominal value, with some points having some overshoot due to controller instabilities that will be explained in Section 4.2. These correspond to the highest and lowest temperature that could be achieved. The fuel inlet temperature was limited by the temperature of the CNG after expanding from the storage tank which is at ambient temperature, and the two-phase flow boundary at the given pressure level.

The data was collected over five hot fire (HF) attempts, of which two were aborted prematurely (HF2 and HF4). The steady-state points that were extracted from the test can be seen in Figure 6. The throttle level is the ratio between the injected mass flow to the nominal mass flow at maximum thrust. The three throttle levels also correspond to three different chamber pressure levels, since these two parameters are approximately linearly proportional.

DOI: 10.13009/EUCASS2025-537

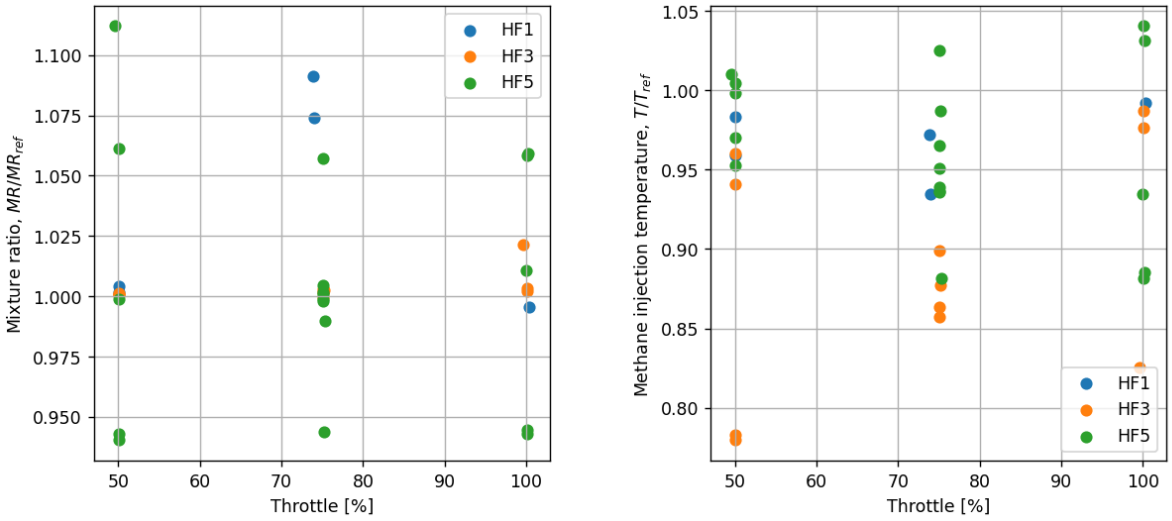

Figure 6: Experimental domain of the test campaign

4.2 Validation of the regenerative cooling model

The predictive capabilities of the calibrated RC model described in Section 3.1 were evaluated by comparing the computed outlet temperature, outlet pressure and pressure drop against experimental measurements. Figure 7 presents the relative error for each predicted variable across all operating points. The outlet pressure predictions show excellent agreement, with deviations within ±1%. Pressure drop predictions fall within ±15%, which is considered good given the relative simplicity of the model and the sensitivity of this metric to the channel roughness which is highly dependent on the printing parameters and build angle. The outlet temperature predictions are also highly accurate, staying within ±5% of the measured values.

The results confirm that the calibrated RC model reliably captures the dominant thermal and hydraulic behavior of the cooling circuit and validates its use for the heat loss corrections applied in the combustion efficiency analysis and as a predictive tool for future design iterations.

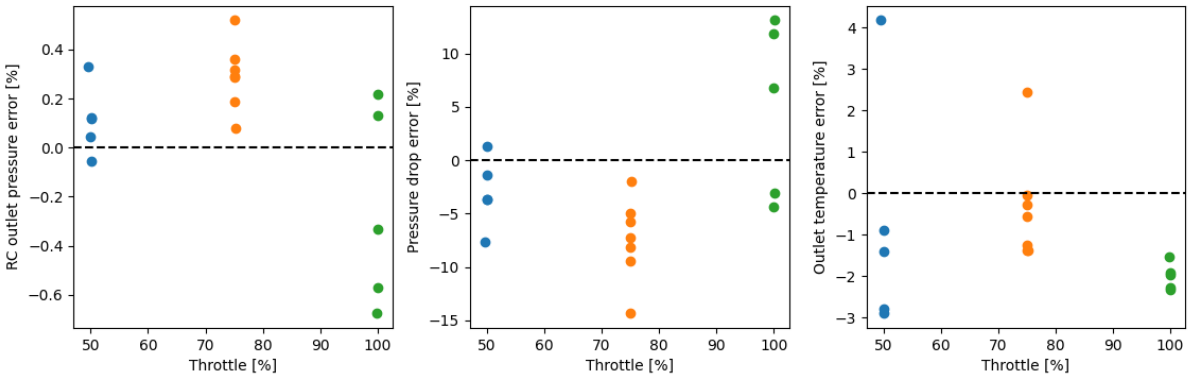

Figure 7: Comparison between the predicted and measured performance of the RC

4.3 Temperature control

The temperature control system was evaluated for its dynamic response and stability. Figure 8 presents a representative test run (HF5), highlighting the transient behaviour observed during the initial phase. The first part of the test has significant oscillations in the fuel temperature, primarily due to two-phase flow conditions in the secondary LNG line but also due to poorly tuned control gains on the mixer valve. These effects lead to oscillations in the mixer valve position and secondary LNG mass flow, which in turn caused fluctuations in the overall fuel temperature and mixture ratio.

Such transients were expected, as the secondary line starts at ambient temperature and must be chilled down by the cold methane flow. In order to remedy this effect, the duration of the first load point of each test was extended with a moderately high secondary LNG mass flow and not considered in the performance analysis. Nevertheless, even after

DOI: 10.13009/EUCASS2025-537

40 seconds in HF5 the temperature of the LNG inlet is still clearly decreasing meaning that the line is not completely cooled down.
Controller parameters were gradually refined between tests, leading to a visible reduction in the amplitude of oscillations between HF1 and HF5. Despite these improvements, complete suppression of thermal instabilities was not achieved. However, once the secondary line approached steady-state thermal condition, stable and repeatable fuel temperatures were consistently observed at the outlet of the mixer at each load point. These stable conditions were critical for isolating the effects of fuel temperature on combustion efficiency in the subsequent analysis.

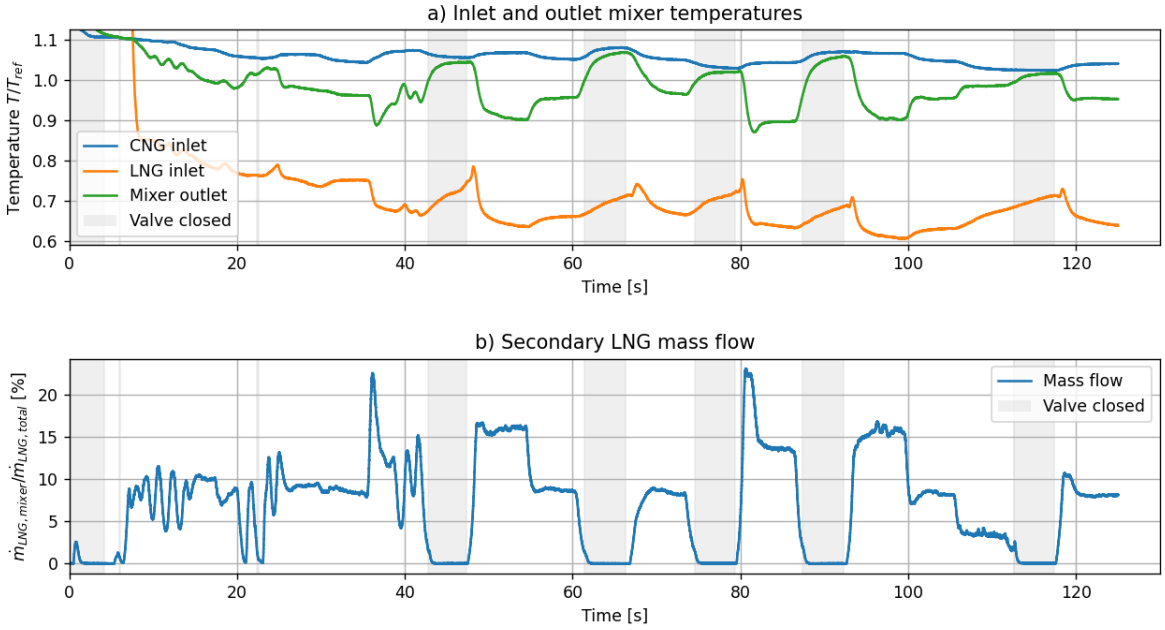

Figure 8: Mixer operation for HF5

4.4 Combustion efficiency trends

Following data collection, the influence of the three primary parameters, total mass flow rate (i.e. throttle), mixture ratio, and methane injection temperature, on the combustion efficiency, η^*, was investigated. To quantify these effects and explore potential nonlinearities and interactions, a second-order linear regression model, including all main effects, squared terms, and pairwise interactions was fitted to the data.
An analysis of the model coefficients revealed that throttle and temperature were highly significant with a significance of $p < 0.001$, as well as their interaction term ($p < 0.02$). In contrast, mixture ratio and all second-order terms were not statistically significant ($p > 0.2$), indicating limited value in capturing the trends over the experimental range.
Based on these insights, a reduced model was constructed that included only the statistically significant terms: linear effects of throttle and temperature and their interaction term. The simplified model maintained a high degree of explanatory power, with an adjusted $R^2 = 0.86$, indicating that over 86% of the variance in η^* is explained despite the reduced complexity.
The comparison between the predictions of the reduced model with the estimated combustion efficiency can be seen in Figure 9. Combustion efficiency was found to increase with higher fuel temperatures and decrease with increasing total mass flow (chamber pressure), ranging from 0.94 at low temperatures and high flow to 1 at low temperatures and low flow across the experimental domain. On the other hand, higher fuel injection temperatures lead to higher combustion efficiencies. If we simplify the equation of state of the methane by the ideal gas, we can state that the fuel velocity is proportional to the temperature, $u_f \propto T$, and the momentum flux is proportional to temperature and mass flow, $\rho u_f^2 \propto T\dot{m}$, since $\rho = P/(RT)$ and $P \propto \dot{m}$. Additionally, by assuming LOX as an incompressible fluid, we derive that the velocity ratio and the momentum flux ratio, often denoted as the J number, are proportional to the term $T/\dot{m}$. Both the velocity ratio and the momentum flux ratio are very common parameters the predict the performance of coaxial injectors, since these terms give an indication of the forces acting on the shear layer which drive the mixing of the propellants [4]. The fact that they are proportional $T/\dot{m}$ explain the trends seen in Figure 9. These trends also suggest that the fuel density, ρ_f, is a strong scalar predictor of combustion efficiency, since $\rho_f \propto \dot{m}/T$, which is the inverse of the previous term.

DOI: 10.13009/EUCASS2025-537

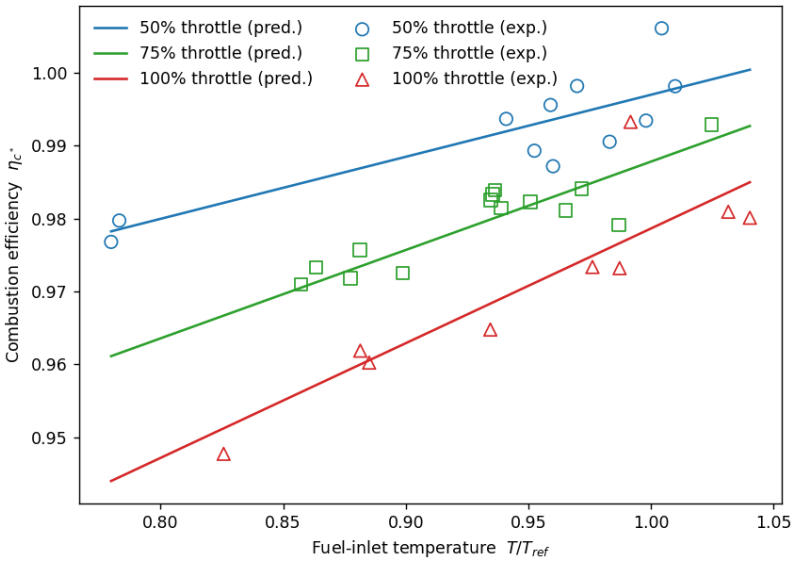

Figure 9: Combustion efficiency vs. temperature at three throttle levels

4.5 Injector characterization via dimensionless parameters

To gain deeper insights into the combustion performance and to be able to compare results with previous and future hardware iterations a similar analysis is performed with key non-dimensional parameters commonly used in rocket injector analysis [4], the Weber number, $We = \rho_f \left(u_f - u_o\right)^2 D/\sigma$, where D is a reference length and σ is the surface tension, and the Reynolds number, $Re = \rho_f u_f D/\mu_f$, where μ_f is the dynamic viscosity.
A first order regression model consisting of these two numbers and their interaction term was also fitted to the data with an adjusted $R^2 = 0.84$. As shown in Figure 10, combustion efficiency increases at low Reynolds numbers, becoming independent of the Weber number when $Re \approx 100\,000$ and reaching values $\eta^* > 0.99$. At higher Reynolds ($Re > 200\,000$) numbers, efficiency improves with increasing Weber number, ranging from $\eta^* = 0.94$, when $We = 35\,000$, to $\eta^* = 0.98$, when $We = 75\,000$.

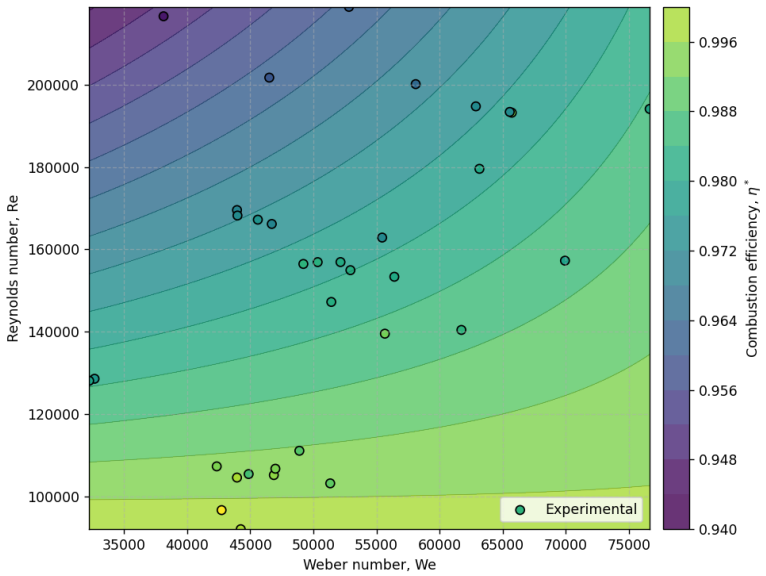

Figure 10: Effect of Weber and Reynold number on combustion efficiency

DOI: 10.13009/EUCASS2025-537

If both numbers are combined, the Ohnesorge number is obtained, which is defined as:

$$Oh = \frac{\sqrt{We}}{Re} = \frac{\mu_f(u_f - u_o)}{\sqrt{\rho_f D\sigma}\, u_f} \tag{4}$$

The above expression can be simplified to $\mu_f/\sqrt{\rho_f D\sigma}$, since $u_f \gg u_o$. As we can see the main term of the Ohnesorge number is the fuel density, ρ_f, which as we have seen before, is a also a good predictor of combustion efficiency because it combines the effects of chamber pressure and fuel injection temperature into one parameter. The key difference between Ohnesorge number and the density is that Oh also combines the surface tension, σ, which is a very impactful parameter for subcritical combustion, and the fuel viscosity, μ_f. Both of these terms are a function of the respective propellant temperatures and provide a more complete picture of the injection.
In Figure 11, we can see the comparison between the relationship of these two parameters with combustion efficiency. First, we can observe that the Ohnesorge number provides a better fit than just the density ($R^2_{Oh} > R^2_{\rho_{fu}}$). Second, the relationship between density and combustion efficiency is a purely linear relationship, which means that for very low densities, the curve would have to be extrapolated and would result in nonphysical predictions of combustion efficiency greater than 1. On the other hand, the Ohnesorge number regression model has a noticeable curvature and it approaches 1 for high Oh.

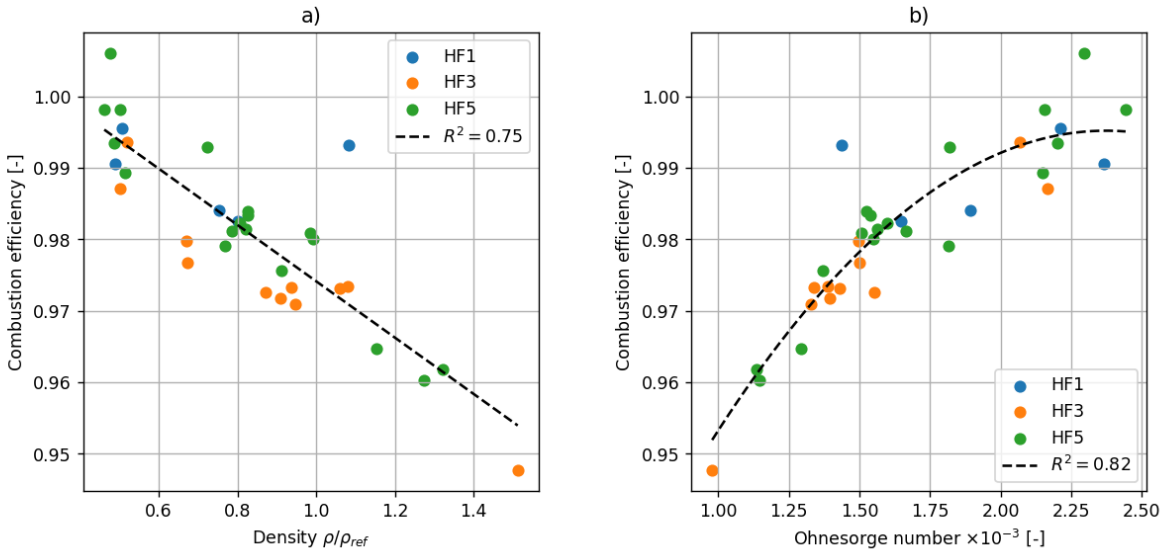

Figure 11: Combustion efficiency vs. fuel density (a); Combustion efficiency vs. Ohnesorge number (b)

The correlations of Figure 10 and Figure 11.b, based on non-dimensional numbers normalized by the injector diameter, have direct implications for injector and cooling system design. Since fuel temperature at injection determines Oh, future injector designs can now be explicitly optimized for the predicted thermal boundary conditions provided by the calibrated regenerative cooling model. This effectively closes the design loop and ensures design compatibility between the injectors and the cooling circuit.

5. Conclusions and Outlook

This paper presented the results of the third hot-fire test campaign of the 15kN LOX/LNG Huracan thrust chamber, focusing on the impact of methane injection temperature on combustion efficiency. A novel propellant feed system was implemented to decouple the injector head from the regenerative cooling loop, allowing precise control of the fuel inlet temperature by blending cryogenic LNG with ambient CNG.
The campaign covered a broad operational envelope across three throttle and mixture ratio settings and multiple fuel temperatures. A 1D regenerative cooling model was calibrated against experimental measurements, showing good predictive accuracy with outlet temperature and pressure deviations within 5% and 1% respectively. This validated model was then used to correct for wall heat losses in the combustion efficiency estimation.

DOI: 10.13009/EUCASS2025-537

Experimental results demonstrated that combustion efficiency increases with fuel injection temperature and decreases with chamber pressure. Regression models using Reynolds, Weber and Ohnesorge numbers showed strong correlation with efficiency, enabling predictive capability for future design iterations.
With the validated regenerative cooling model and the predictive combustion efficiency correlations, the design loop is now effectively closed. This enables the development of a new regenerative cooling architecture with improved confidence in predicting fuel outlet temperatures. As a result, the injector can be re-optimized specifically for the expected thermal boundary conditions, ensuring alignment between cooling and combustion performance. The next test campaign will focus on validating a new design iteration based on these models and expanding the scope toward other critical performance aspects, such as combustion stability.

References

[1] Stimpson, C., J. Snyder, K. Thole and D. Mongillo. 2016. Scaling Roughness Effects on Pressure Loss and Heat Transfer of Additively Manufactured Channels. *Journal of Turbomachinery*. 139. 10.1115/1.4034555.
[2] Deeken, J. 2014. Experimentelle Untersuchungen zu neuartigen, porösen Injektoren für den Einsatz in kryogenen Hochdruck-Raketenantrieben. PhD Thesis. DLR-Forschungsbericht. Universität Stuttgart
[3] Pizzarelli, M. 2008. Modelling of cooling channel flow in liquid-propellant rocket engines. PhD Thesis. Sapienzia University.
[4] Sutton, G.P. and O. Biblarz. 2001. Rocket Propulsion Elements. 7th Edition, John Wiley, Hoboken.
[5] Goodwin, D., H. Moffat, I. Schoegl, R. Speth and B. Weber 2024. Cantera: An object-oriented software toolkit for chemical kinetics, thermodynamics, and transport processes. https://www.cantera.org, Version 3.1.0. doi:10.5281/zenodo.14455267
[6] Incropera, F. and D. DeWitt. 2007. Fundamentals of Heat and Mass Transfer, 6th Edition, J. Wiley & Sons, New York
[7] Powell, W. 1973. Simplified Procedures for Correlation of Experimentally Measured and Predicted Thrust Chamber Performance. NASA Technical Memorandum 33-548
[8] Gordon S., B. McBride. 1994. Computer Program for Calculation of Complex Chemical Equilibrium Compositions and Applications. I. Analysis. NASA Reference Publication 1311
[9] Gordon, S. 1988. Finite Area Combustor Theoretical Rocket Performance. NASA Technical Memorandum 100785
[10] Lemmon, E., I. Bell, M. Huber, and M. McLinden 2018. NIST Standard Reference Database 23: Reference Fluid Thermodynamic and Transport Properties-REFPROP, Version 10.0, National Institute of Standards and Technology, Standard Reference Data Program, Gaithersburg
[11] Schack, A. 1953. Der Industrielle Wärmeübergang für Praxis Und Studium Mit Grundlegenden Zahlenbeispielen. 4th Edition, Dusseldorf
[12] Bartz, D. 1957. A Simple Equation for Rapid Estimation of Rocket Nozzle Convective Heat Transfer coefficients. *Journal of Jet Propulsion* 27, no. 1 (1957): 49–53. https://doi.org/10.2514/8.12572.
[13] Crachi, M., T. Cruz, M. Strixner, A. Bee, R. Mabboux, W. Armbruster, and R. Sesana. 2024. A novel multifunctional additive manufactured lattice structure design for thermal and mechanical improvement of liquid rocket engine injector face plates. In: 9th *Edition of the 3AF International Conference on Space Propulsion*
[14] Bee, A., T. Cruz, M. Crachi, M. Strixner, W. Armbruster, M. Börner, J. Hardi, R. Mabboux P. Vinet and S. Reichstadt. 2024. Design, Development and Testing of the Injector for a 3D-Printed Throttleable and Reusable LOX/Methane Rocket Engine. In: 9th *Edition of the 3AF International Conference on Space Propulsion*
[15] Crachi, M., T. Cruz, J. Matt, P. Vinet, S. Matteini, Y. Torres, R. Santos, W. Armbruster. 2025. Experimental characterization of the cycling thermo-mechanical behaviour of a reusable LOX-LNG regeneratively cooled thrust chamber. In: 11th *Edition of the European Conference for AeroSpace Sciences (EUCASS)*